CLINICAL INVESTIGATIVE STUDY

JOURNAL OF
NEUROIMAGING
THE OFFICIAL JOURNAL OF THE AMERICAN SOCIETY OF NEUROIMAGING

WILEY

Applicability of multiple quantitative magnetic resonance methods in genetic brain white matter disorders

Menno D. Stellingwerff[1,#] | Murtadha L. Al-Saady[1,#] | Kwok-Shing Chan[2] |
Adam Dvorak[3] | José P. Marques[2] | Shannon Kolind[3] |
Stefan D. Roosendaal[4] | Nicole I. Wolf[1] | Frederik Barkhof[4,5] |
Marjo S. van der Knaap[1,§] | Petra J. W. Pouwels[4,§]

[1]Department of Child Neurology, Amsterdam Leukodystrophy Center, Emma Children's Hospital, Cellular & Molecular Mechanisms, Amsterdam University Medical Centers, and Amsterdam Neuroscience, Vrije Universiteit, Amsterdam, Netherlands

[2]Donders Institute for Brain, Cognition and Behaviour, Radboud University, Nijmegen, Netherlands

[3]Department of Physics and Astronomy, University of British Columbia, Vancouver, British Columbia, Canada

[4]Department of Radiology and Nuclear Medicine, Amsterdam University Medical Centers, and Amsterdam Neuroscience, Amsterdam, Netherlands

[5]Institutes of Neurology and Healthcare Engineering, University College London, London, UK

Correspondence
Petra J. W. Pouwels, Amsterdam University Medical Center, De Boelelaan 1117, 1081 HV Amsterdam, Netherlands.
Email: pjw.pouwels@amsterdamumc.nl

[§]Marjo S. van der Knaap and Petra J. W. Pouwels share the senior authorships.

Abstract

Background and purpose: Magnetic resonance imaging (MRI) measures of tissue microstructure are important for monitoring brain white matter (WM) disorders like leukodystrophies and multiple sclerosis. They should be sensitive to underlying pathological changes. Three whole-brain isotropic quantitative methods were applied and compared within a cohort of controls and leukodystrophy patients: two novel myelin water imaging (MWI) techniques (multi-compartment relaxometry diffusion-informed MWI: MCR-DIMWI, and multi-echo T2 relaxation imaging with compressed sensing: METRICS) and neurite orientation dispersion and density imaging (NODDI).

Methods: For 9 patients with different leukodystrophies (age range 0.4-62.4 years) and 15 control subjects (2.3-61.3 years), T1-weighted MRI, fluid-attenuated inversion recovery, multi-echo gradient echo with variable flip angles, METRICS, and multi-shell diffusion-weighted imaging were acquired on 3 Tesla. MCR-DIMWI, METRICS, NODDI, and quality control measures were extracted to evaluate differences between patients and controls in WM and deep gray matter (GM) regions of interest (ROIs). Pearson correlations, effect size calculations, and multi-level analyses were performed.

Results: MCR-DIMWI and METRICS-derived myelin water fractions (MWFs) were lower and relaxation times were higher in patients than in controls. Effect sizes of MWF values and relaxation times were large for both techniques. Differences between patients and controls were more pronounced in WM ROIs than in deep GM. MCR-DIMWI-MWFs were more homogeneous within ROIs and more bilaterally symmetrical than METRICS-MWFs. The neurite density index was more sensitive in detecting differences between patients and controls than fractional anisotropy. Most measures obtained from MCR-DIMWI, METRICS, NODDI, and diffusion tensor imaging correlated strongly with each other.

Conclusion: This proof-of-concept study shows that MCR-DIMWI, METRICS, and NODDI are sensitive techniques to detect changes in tissue microstructure in WM disorders.

KEYWORDS

brain, MCR-DIMWI, metrics, myelin water imaging, NODDI, tissue microstructure

INTRODUCTION

Leukodystrophies constitute a large and highly heterogeneous group of genetic diseases primarily affecting various components of the white matter (WM) of the central nervous system, including myelin, axons and neurites, oligodendrocytes, astrocytes, microglia, blood vessels, and extracellular matrix.[1] Conventional magnetic resonance imaging (MRI) plays a central role in diagnosis through pattern recognition and may be used in volumetric analyses or visual rating scales. However, signal abnormalities on conventional MRI lack specificity regarding the underlying microstructural changes. For monitoring patients, imaging techniques should ideally be quantitative and extract information on specific pathological processes.

Novel MRI sequences with appropriate postprocessing algorithms can provide quantitative measures reflecting various microstructural components.[2,3] Myelin content can be indirectly estimated using myelin water imaging (MWI) techniques, such as multi-echo T2 relaxation imaging with compressed sensing (METRICS) and multi-compartment relaxometry-diffusion informed MWI (MCR-DIMWI). Both techniques exploit differences in the relaxation times of water in different compartments to distinguish myelin water from water residing in other compartments.[4,5] Neurite density can be estimated with methods using multi-shell diffusion-weighted imaging (DWI) data, for instance, neurite orientation dispersion and density imaging (NODDI).[6]

In this paper, we explore the potential applicability of METRICS, MCR-DIMWI, and NODDI in the context of leukodystrophies. We describe the acquisition, which is feasible for clinical applications, and the analysis pipeline to extract quantitative measures from selected regions of interest (ROIs). We compare the three techniques and investigate whether they are effective in discerning patients with leukodystrophies from controls.

METHODS

Participants

The study was approved by the local ethics committee and informed consent was obtained from subjects and/or their parents. Patients had genetically confirmed leukodystrophy and WM signal abnormalities on conventional imaging (details in Table 1). Control subjects were either previous control participants in leukodystrophy research, or were scanned because of neurological complaints, such as headache/migraine, long-standing vomiting, or syncope, without a specific diagnosis. MRI scans of control subjects were excluded if any abnormalities were present on conventional imaging. To get an impression of between-scanner variability, one additional 33-year-old healthy control subject was scanned within 1 day on all three scanners (see below).

MRI acquisition

All subjects were examined on 3 T whole-body MR scanners (either Ingenia Elition X [scanner 1] or Ingenia [scanner 2&3]; Philips Medical Systems) using a 32-channel head coil. All patients were scanned on scanner 1, control scans were acquired on either of the three scanners (Table 1). The applied sequences are summarized in Table 2. Conventional imaging included 3-dimensional (3D) T1 and 3D fluid-attenuated inversion recovery (FLAIR). The sequences multi-shell DWI, multi-echo gradient echo with variable flip angles (MGRE-VFA), and METRICS were all obtained with 2.5-mm isotropic resolution to reduce acquisition time while ensuring high signal-to-noise ratio (SNR). All sequences were obtained in oblique transverse orientation, apart from 3D T1 and METRICS, which were obtained in sagittal orientation.

Multi-shell DWI was obtained with single spin-echo echo-planar images. Using a multiband acceleration factor 2, a total of 97 volumes (9b0, 29b1000, 59b2000, sampled and interleaved according to Caruyer et al.)[7] were obtained. On scanner 3 without multiband functionality, we acquired a total of 54 volumes (6b0, 16b1000, 32b2000). To allow correction for susceptibility-induced geometrical distortion, we acquired two volumes with reversed phase-encoding and without diffusion encoding.

3D MGRE-VFA was obtained in one sequence, using a home-developed patch, to ensure constant transmit and receive gains. Acquiring a wide range of flip angles improves the fit of MCR-DIMWI. The flip angle order was based on placing the most important flip angles needed for T1 determination at the start of the sequence, as potential subject movement during scanning is more often seen toward the end of the acquisition.[8] For B1 mapping, a fast B1-DREAM sequence was applied.[9] 3D METRICS was obtained with a turbo spin echo sequence, as described.[5] For both MGRE-VFA and METRICS, we kept the reconstructed voxel size identical to the acquired voxel size to limit the computational time during analyses.

TABLE 1 Subject inclusion and characteristics.

	Controls (n = 15)	Leukodystrophy patients (n = 9)
Diagnosis (n)	Not applicable	Aicardi-Goutières syndrome (4) Alexander disease (2) Oculodentodigital dysplasia (2) Zellweger spectrum disorder (1)
Male (n [%])	7 [47%]	5 [56%]
Age in years (median [range])	23.5 [2-61]	9 [0.4-62]
Scanner (n)	Scanner 1 (7) Scanner 2 (2) Scanner 3 (6)	Scanner 1 (9)
Performed under anesthesia (n [%])	4 [27%]	6 [67%]

Abbreviation: n, number.

TABLE 2 Acquisition protocol.

Sequence	AT	Timing parameters (ms)	Acq. voxel size (mm^3)	Rec. voxel size (mm^3)	Other characteristics	Quantitative measures
3D T1-weighted FFE	4min14s	TR = 9.1; TI = 1130; TE = 4.2	0.9×0.9×0.9	0.5×0.5×0.9	Flip angle = 8°; SENSE acceleration 2.5×	
3D FLAIR	5min2s	TR = 4800; TI = 4650; TE = 356	1.0×1.0×1.0	0.8×0.8×0.8	Compressed SENSE acceleration 6.5x	
Multi-shell DWI[a]			2.5×2.5×2.5	2.5×2.5×2.5	SENSE acceleration 1.5×	FA; NDI; ODI; FISO
Scanner 1	6min35s	TR = 3760; TE = 95			multiband 2; 9b0, 29b1000, 59b2000	
Scanner 2	7min56s	TR = 4580; TE = 95			multiband 2; 9b0, 29b1000, 59b2000	
Scanner 3	7min56s	TR = 7700; TE = 95			no multiband; 6b0, 16b1000, 32b2000	
B1-DREAM	12s	TR = 6.6; TE = 1.3				
Multi-GRE with VFA	10min5s	TR = 46 12 TEs 2.15-35.70 ΔTE 3.05	2.5×2.5×2.5	2.5×2.5×2.5	Flip angle = 70°, 20°, 10°, 30°, 40°, 50°, 5°	MWF; T1; T2*
METRICS	9min27s	TR = 1066 56 TEs 7-392 ΔTE 7	2.5×2.5×2.5	2.5×2.5×2.5	Compressed SENSE acceleration 10x	MWF; IET2

Abbreviations: Acq, acquired; AT, acquisition time; 3D, 3-dimensional; DREAM, dual refocusing echo acquisition mode; DWI, diffusion-weighted imaging; FA, fractional anisotropy; FFE, fast field echo; FISO, free water fraction; FLAIR, fluid-attenuated inversion recovery; GRE, gradient echo; IET2, geometrical mean of the intra- and extra-axonal T2; METRICS, multi-spin echo T2 relaxation imaging with compressed sensing; min, minutes; mm, millimeter; ms, milliseconds; MWF, myelin water fraction; NDI, neurite density index; ODI, orientation dispersion index; Rec, reconstructed; s, seconds; SENSE, sensitivity encoding; TE, echo time; TI, inversion time; TR, repetition time; VFA, variable flip angle.
[a]DWI acquisition parameters differed per scanner. Voxel size and SENSE acceleration are identical at all scanners. AT includes volumes with reversed phase-encoding for geometrical correction.

MRI analysis pipeline

Postprocessing

An overview of the pipeline is shown in Figure 1. DICOM data were converted to nifti-format using dcm2niix (MRIcroGL 2019, Columbia, South Carolina, USA).[10] Synthseg (version 2.0, London, UK)[11] was used to segment the 3D T1 into anatomical WM, cortical gray matter (GM), deep GM, and cerebrospinal fluid (CSF) ROIs. After visual quality control, manual correction of the segmented images was performed when needed. The intracranial volume was defined as brain tissue plus CSF. A single volume of the MGRE-VFA, METRICS, and multi-shell
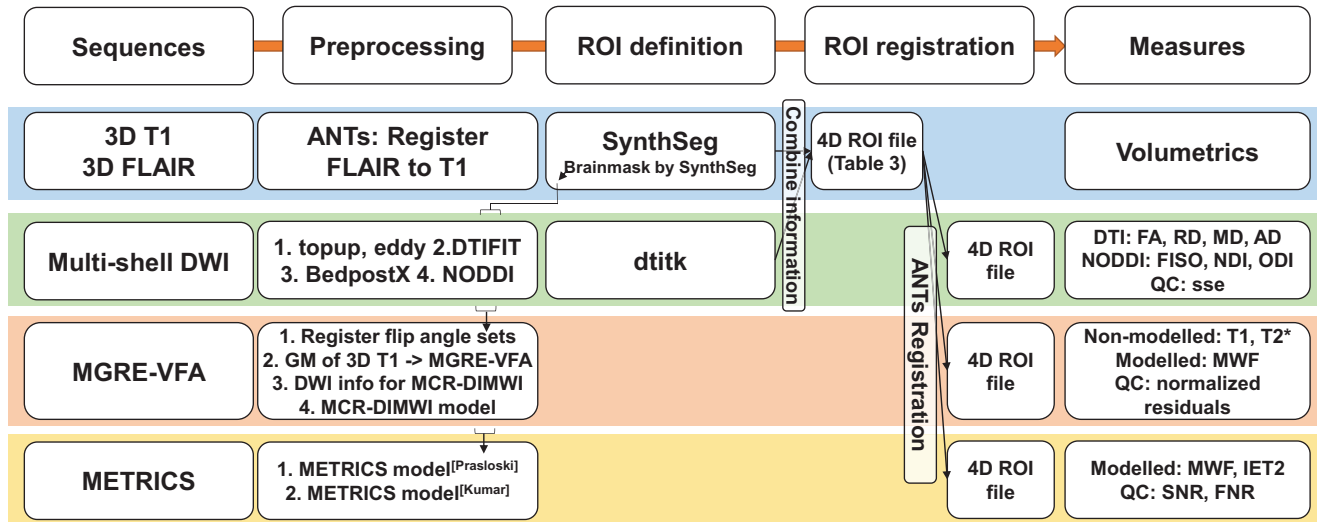
FIGURE 1 Flow-chart representing the current analysis pipeline. 3D T1 images are segmented using SynthSeg,[11] which also provides a brain mask and a GM-mask. Multi-echo gradient echo with variable flip angles (MGRE-VFA) and multi-echo T2 relaxation imaging with compressed sensing (METRICS) are processed according to Chan and Marques,[4] and Prasloski et al./Kumar et al.[17,18] For multi-shell diffusion-weighted imaging (DWI) data, various postprocessing steps are taken as described. To define regions of interest (ROIs), both the SynthSeg-derived ROIs and the dtitk-derived ROIs are combined and merged into a final 4D ROI file (see Table 3). The masks from 3D T1 space are registered to multi-shell DWI, MGRE-VFA, and METRICS space. Ultimately, the quantitative measures are extracted using the individual ROIs as masks. Abbreviations: AD, axial diffusivity; ANTs, advanced normalization tools; 3D, 3-dimensional; 4D, 4-dimensional; DTI, diffusion tensor imaging; FA, fractional anisotropy; FISO, free water fraction; FLAIR, fluid-attenuated inversion recovery; FNR, fit-to-noise ratio; GM, gray matter; IET2, geometrical mean of the intra- and extra-axonal T2; MCR-DIMWI, multi-compartment relaxometry-diffusion informed myelin water imaging; MD, mean diffusivity; MWF, myelin water fraction; NDI, neurite density index; NODDI, neurite orientation dispersion and density imaging; ODI, orientation dispersion index; QC, quality control; RD, radial diffusivity; SNR, signal-to-noise ratio; sse, sum of squared errors.

DWI was registered to 3D T1 space using Advanced Normalization Tools (ANTs, version 2.3.5, Pennsylvania, Philadelphia, USA),[12] and the inverse transformation was used to obtain an intracranial volume mask in MGRE-VFA, METRICS, and multi-shell DWI spaces.

Multi-shell DWI data were corrected using topup and eddy with outlier replacement from FMRIB's Software Library (FSL, version 6.0.4, Oxford, UK).[13,14] BedpostX was performed for subsequent use of diffusion data in MCR-DIMWI. NODDI analyses were based on the Watson model and performed with the CUDA Diffusion Modelling Toolbox (version 9.1, Oxford, UK).[15] Quantitative values of NODDI include: neurite density index (NDI), orientation dispersion index (ODI), and the free (isotropic) water fraction (FISO). The diffusion tensor imaging (DTI) tensor was calculated for the b0-b1000 shell using DTIFIT, as these b-values are most often used clinically. For this paper, we only report fractional anisotropy (FA) as an example of a conventional DTI measure that is often reported alongside (and compared) with NODDI measures. Other measures from the diffusion tensor can be extracted with the same pipeline, but to limit the amount of measures and analyses, these are not reported in the current manuscript. A goodness-of-fit is given by the sum-of-squared errors (SSE), and a lower SSE indicates a better fit.

MGRE-VFA was processed according to the MCR-DIMWI pipeline, including all assumptions and fixed parameters as described by Chan and Marques (code accessible through: https://github.com/kschan0214).[4] Motion between flip angles was corrected by coreg-istering all flip angle volumes to the first volume, using the ANTs transformations of the shortest echo time (TE) volumes.[12] To adjust the median of the phase of the first brain-masked image to zero, a phase-shift was added to all phase images. This ensured a quasi-linear phase evolution along all TEs and prevented artifacts arising from the significant eddy currents on the first echo time. The quantitative measure from MCR-DIMWI is myelin water fraction (MWF). A goodness-of-fit is given by a normalized residual, and a lower residual indicates a better fit. Voxels with residuals exceeding a threshold of "median + 3 times the interquartile range (IQR)" within the brain mask were considered inaccurate and were excluded from the quantitative analyses. In addition, we estimated quantitative maps with single-compartment T1 values using despot1 (using all flip angles and the shortest TE)[16] and T2* (using the volumes with flip angle 20 and all TEs).

METRICS was processed using two methods. One method is described by Prasloski et al.[17] The other method is described in more detail by Kumar and uses spatial smoothness constraints with respect to flip angle inhomogeneity to improve noise robustness.[18] Both analyses used 90 logarithmically spaced T2-values between 5 and 10,000 milliseconds. Myelin water was defined as having a T2-relaxation time between 10 and 40 milliseconds, and intra- and extra-axonal water as having a T2-relaxation time between 40 and 200 milliseconds. Quantitative measures from METRICS include the MWF and the geometrical mean of the intra- and extra-axonal

TABLE 3 Available regions of interest.

ROIs	GM/WM/CSF	L/R	ROIs	WM tract	L/R
Cerebrum	Cortical GM/WM	L/R	Anterior commissure	WM tract	
Cerebellum	Cortical GM/WM	L/R	Arcuate fasciculus	WM tract	L/R
Frontal lobe	Cortical GM/WM	L/R	Frontal aslant tract	WM tract	L/R
Occipital lobe	Cortical GM/WM	L/R	Cingulum	WM tract	L/R
Parietal lobe	Cortical GM/WM	L/R	Forceps major	WM tract	
Temporal lobe	Cortical GM/WM	L/R	Forceps minor	WM tract	
Brainstem	Mixed GM&WM		Corpus callosum	WM tract	
Caudate	Deep GM	L/R	Middle of corpus callosum	WM tract	
Pallidum	Deep GM	L/R	Corticospinal tract	WM tract	L/R
Putamen	Deep GM	L/R	Fornix	WM tract	
Thalamus	Deep GM	L/R	Frontopontine	WM tract	L/R
Accumbens area	Deep GM	L/R	Inferior cerebellar peduncle	WM tract	L/R
Amygdala	Deep GM	L/R	Inferior frontooccipital fasciculus	WM tract	L/R
Hippocampus	Deep GM	L/R	Inferior longitudinal fasciculus	WM tract	L/R
Ventral diencephalon	Mixed GM&WM	L/R	Middle cerebellar peduncle	WM tract	
Lateral ventricle	CSF	L/R	Middle longitudinal fasciculus	WM tract	L/R
Inferior lateral ventricle	CSF	L/R	Medial lemniscus	WM tract	L/R
3rd ventricle	CSF		Occipitopontine tract	WM tract	L/R
4th ventricle	CSF		Optic radiation	WM tract	L/R
Peripheral CSF	CSF		Parietopontine tract	WM tract	L/R
			Superior cerebellar peduncle	WM tract	
			Superior longitudinal fasciculus	WM tract	L/R
			Spinothalamic tract	WM tract	L/R
			Uncinate fasciculus	WM tract	L/R
			Vertical occipital fasciculus	WM tract	L/R

Note: L/R (left/right) indicates bilaterally available regions of interest (ROIs), cortical GM/WM indicates the availability of separate white matter and cortical gray matter ROIs.
Abbreviations: CSF, cerebrospinal fluid; GM, gray matter; L, left; R, right; WM, white matter.

T2 (IET2). A goodness-of-fit is given by a fit-to-noise ratio (FNR), as described by Dvorak et al.,[5] and a higher FNR indicates a better fit.

ROI selection

Using the single shell (b0-b1000) tensors, a dtitk-group template was created based on control data, as described before.[19–21] Subsequently, individual patient tensors were registered to the group template. Transformations between subject space and group space and between group space and IIT space (atlas space of Illinois Institute of Technology) were combined to allow a single transformation from subject DWI space to IIT space and vice versa.[22]

The IIT atlas was also registered to MNI space (atlas space of Montreal Neurological Institute) as implemented in FSL. The SynthSeg segmentations were combined with the MNI brain atlas to define WM and cortical GM within the cerebral lobes. SynthSeg-derived deep GM ROIs (see Table 3 for a full list of structures) were eroded to prevent partial volume effects with surrounding tissue or CSF. Probabilistic WM tracts from the IIT atlas were registered to subject T1 space using the available transformations, and voxels were confined to the SynthSeg WM mask.

All ROIs were coregistered to subject multi-shell DWI, MGRE-VFA, and METRICS space. Within the subject space, the medians of quantitative measures within ROIs were extracted, because distributions can be skewed and to limit the influence of potential outliers. In addition, we determined the within-ROI coefficient of variance (COV), defined as (standard deviation [SD]/mean)*100%, as a measure of the homogeneity within an ROI. For the probabilistic WM tracts, weighted means were extracted. A list of all available ROIs and WM tracts within our pipeline is shown in Table 3, further referred to as ROIs. For this paper, we selected a subset of ROIs (ie, frontal WM, temporal WM, parietal WM, occipital WM, corticospinal tract, tracts through the corpus callosum, thalamus, putamen, and caudate nucleus) for illustrative purposes.
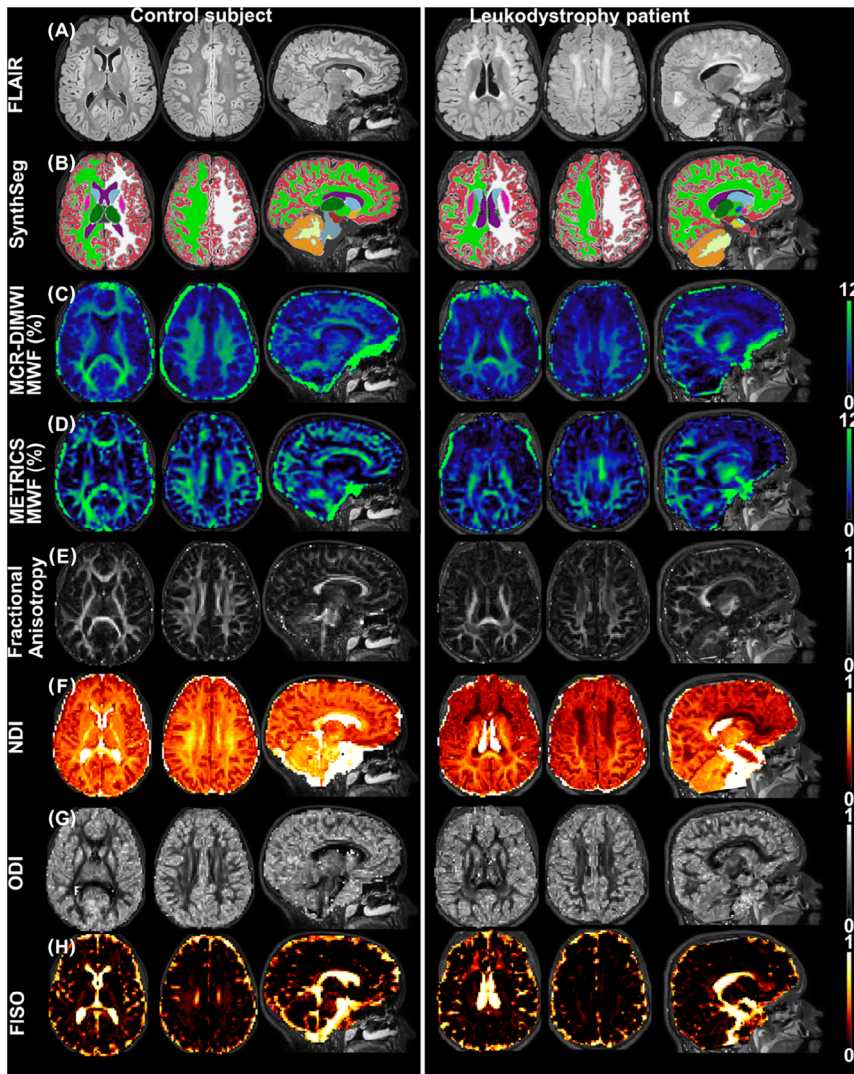
FIGURE 2 Fluid-attenuated inversion recovery (FLAIR), SynthSeg segmentation of cerebral and cerebellar WM and cortex, and deep gray matter, maps of myelin water fraction (MWF) obtained from multi-compartment relaxometry-diffusion informed myelin water imaging (MCR-DIMWI) and multi-echo T2 relaxation imaging with compressed sensing (METRICS, postprocessing according to Kumar et al.)[18] fractional anisotropy (FA), and neurite orientation dispersion and density imaging (NODDI) measures neurite density index (NDI), orientation dispersion index (ODI), and free water fraction (FISO) in a control subject (aged 11 years) and a patient with a leukodystrophy (aged 12 years). (A, B) Patient FLAIR shows WM hyperintensities mainly in the frontal WM, which are segmented as WM. (C, D) Both myelin water imaging techniques show lower MWF in the corresponding areas. Both techniques also contain some hyperintense (bright green) artifacts mainly at the orbitofrontal rim of the brain. (E-H) FA is decreased in the abnormal WM, which is also shown by NODDI as lower NDI and higher FISO values. Effects on ODI are less evident.

Statistical analysis

All analyses were performed in RStudio software (version 1.1.463; RStudio Team). Means and SDs are reported, based on all subjects or on control subjects and leukodystrophy patients separately. The laterality index (LI) was calculated based on values within left (L) and right (R) ROIs as (L−R)/(L+R). An LI approximating 0 indicates a small left-right asymmetry. As data of multiple ROIs were extracted per subject, we used multilevel analyses with subject as a clustering variable. Age at the time of MRI was used as a covariate. Multiple-comparison correction was performed according to Holm. A p-value below .05 was considered indicative of a statistically significant difference. The interaction effect between group and ROI was also investigated using multilevel analyses, including its effect size expressed as partial eta squared (η_p^2). Effect sizes are small for $\eta_p^2 = 0.01$, medium for $\eta_p^2 = 0.06$, and large for $0.14 \leq \eta_p^2 \leq 1.0$.[23] For the between-scanner comparison, the COV was estimated based on SD and mean of ROI values observed on each of the three scanners.

RESULTS

Visual results

3D FLAIR images of a control subject and a patient with leukodystrophy are shown in Figure 2A. 3D T1 images of all subjects were successfully segmented by SynthSeg. Segmentation examples are shown in Figure 2B. Abnormal and normal-appearing white matter (NAWM) as seen on FLAIR were both identified as WM by SynthSeg (white and lime green areas in the left and right hemispheres). MWF maps throughout the brain were obtained with MCR-DIMWI and METRICS (Figure 2C,D). Visual comparison showed that both techniques depicted lower MWF values in the affected frontal WM in the patient than in the control subject. Unrealistically high MWF was commonly observed at the border of orbitofrontal and temporal regions in MCR-DIMWI due to the strong signal dephasing arising from the large susceptibility differences between tissue and air (Figure 2C). These areas were typically identified as outliers with high normalized

residuals and excluded from the ROIs, leading to the exclusion of at most 2% and 3% of voxels in frontal and temporal WM ROIs, respectively. In METRICS, unrealistically high MWF was commonly observed in areas with CSF or venous blood flow and in deep GM areas. The affected WM in the patient was also characterized by lower values of FA and NDI and higher FISO, whereas ODI did not show clear differences (Figure 2E-H).

Quantitative quality assessment

In the comparison of the two METRICS postprocessing methods,[17,18] the MWF- and IET2-values derived with the Kumar algorithm including spatial smoothness constraints had a significantly lower within-ROI COV than those of the original Prasloski version (Table 4), indicating a more homogeneous distribution within ROIs (MWF: $F(168) = 13.8$, $p < .001$; IET2: $F(168) = 74.8$, $p < .001$). For this paper, we, therefore, present measures obtained with the algorithm including spatial correlations.

The within-ROI COV was larger for METRICS than for MCR-DIMWI ($F(167) = 14.8$, $p < .001$), which indicates that the MCR-DIMWI-derived MWF values were more homogeneous per ROI (Table 4). For patients, the difference was prominent in all ROIs, and for controls mainly in deep GM. The normalized residuals of MCR-DIMWI were lowest in parietal WM (Table 5), and higher in deep GM ROIs. FNR and SNR of METRICS were highest in WM ROIs (reaching values around 500), and lowest in the caudate nucleus and thalamus.

For all quantitative measures, there was a strong agreement between the left and right hemispheres, as indicated by mean LI-values near 0, both for control subjects and patients (Table 6). A low between-subject SD for IET2, NDI, ODI, and FA indicated that the LI of these measures was small for all subjects. The SD was higher for the two MWF measures than for most other quantitative measures, indicating larger within-subject left-right variations in MWF values. This was observed especially in deep GM areas. In general, left-right variations were higher for METRICS than for MCR-DIMWI. In WM ROIs, these differences were mostly seen in the patient group, in deep GM, the differences were notable for both patients and controls. For FISO, large left-right variations were observed, due to the fact that in many subjects and ROIs, the value of FISO was (near) 0, limiting the interpretation of LI.

The between-scanner comparison based on one healthy control showed the lowest COVs for IET2 and T2* (Table 7). COVs for METRICS-MWF were smaller than for MCR-DIMWI-MWF. COVs for WM ROIs were lower than for deep GM ROIs.

Relaxometry methods

Both MCR-DIMWI and METRICS detected lower MWF of cerebral WM in patients than in controls (MCR-DIMWI $F(1,21) = 66.4$, $p < .001$; METRICS $F(1,21) = 55.1$, $p < .001$) (Figure 3). An increase of MWF with age was seen in controls (MCR-DIMWI

$F(1,13) = 18.9$, $p < .001$; METRICS $F(1,13) = 20.9$, $p < .001$). The techniques corresponded well regarding MWF values in most ROIs, although METRICS tended to yield higher values ($F(1,175) = 25.8$, $p < .001$), and the slopes of the correlation differed per ROI (ROI*method interaction effect $F(8,175) = 2.50$, $p = .01$) (Figure 4).

As the three subjects younger than 2 years had much lower MWF values, probably partly due to incomplete myelination, we decided not to include these patients in quantitative comparisons between patients and controls. Table 8 shows mean MWF values per region obtained with both techniques for all subjects above the age of 2 years. As already graphically displayed in Figure 4, differences in MWF between patients and controls were most prominent in WM ROIs (ROI*group interaction effect MCR-DIMWI $F(8,152) = 11.9$, $p < .001$; METRICS $F(8,152) = 8.8$, $p < .001$). Overall effect sizes were large for both MWF techniques (partial $\eta^2 = 0.38$ for MCR-DIMWI MWF, and 0.32 of METRICS MWF). Table 8 shows the METRICS-derived IET2 and the single-compartment relaxation times T1 and T2* from the VFA-MGRE data. Relaxation times were generally higher in patients than controls (see also Figure 3), again mainly in WM ROIs (T1 $F(8,152) = 24.1$, $p < .001$; T2* $F(8,152) = 3.0$, $p = .004$; IET2 $F(8,152) = 6.2$, $p < .001$), with large overall effect sizes for T1 and IET2, and a medium effect size for T2*.

Multi-shell DWI data

Table 8 shows the mean FA and NODDI values per ROI in all subjects above the age of 2 years. Both FA and NDI differed significantly between controls and patients (ROI*group interaction effect FA $F(8,152) = 8.8$, $p = <.001$, NDI $F(8,152) = 11.7$, $p < .001$), and overall effect sizes were large for both measures (see also Figure 3). In the post-hoc analysis, FA was only significantly lower in patients in the tracts through the corpus callosum, while NDI was lower in more WM ROIs. FISO and ODI showed similar values in controls and patients. Based on measures of all selected ROIs from all controls and patients, Figure 5 shows the relation between NDI and FA, which is partly influenced by the ODI. For each ODI range, NDI correlated strongly with FA.

Comparing multi-shell DWI and relaxometry techniques

To illustrate the relation between the various quantitative measures, Figure 6 shows MCR-DIMWI, METRICS, multi-shell DWI, and DTI-derived measures in one arbitrarily selected ROI, the left parietal WM, for all controls and patients. Correlations were observed between MWF, T1, T2*, IET2, FA, and NDI. ODI hardly correlated with the other quantitative measures, and within this ROI, only negatively correlated with MCR-DIMWI MWF values in the group of patients. Similar correlations were observed in the other WM ROIs. Deep GM ROIs also showed comparable, though weaker, correlations (data not shown).

TABLE 4 Coefficients of variance within regions of interest.

		MCR-DIMWI	METRICS[D]		METRICS[K]		DTI	NODDI		
		MWF COV	MWF COV	IET2 COV	MWF COV	IET2 COV	FA COV	NDI COV	ODI COV	FISO COV
WM ROIs										
Cerebral WM	CON	41.3 ± 4.1	55.4 ± 7.2	7.1 ± 0.6	44.8 ± 10.7	4.5 ± 0.5	55.8 ± 2.4	23.0 ± 2.0	48.5 ± 1.7	184.3 ± 53.3
	PAT	54.0 ± 13.8	88.2 ± 17.6	12.1 ± 4.1	99.0 ± 40.9	7.7 ± 2.9	52.6 ± 3.6	28.6 ± 9.6	46.9 ± 3.0	250.3 ± 52.3
Frontal WM	CON	40.4 ± 4.6	53.4 ± 10.2	6.7 ± 0.5	45.0 ± 13.1	4.4 ± 0.7	55.0 ± 2.6	22.8 ± 2.2	45.9 ± 2.2	187.2 ± 70.1
	PAT	50.3 ± 16.8	88.2 ± 19.0	11.9 ± 5.6	100.8 ± 43.1	6.8 ± 2.5	50.3 ± 2.8	30.3 ± 15.6	44.6 ± 4.5	248.0 ± 67.8
Parietal WM	CON	41.5 ± 4.6	52.3 ± 8.9	6.5 ± 1.0	41.0 ± 13.5	3.8 ± 0.7	55.4 ± 4.0	22.3 ± 2.5	48.1 ± 1.5	165.3 ± 48.9
	PAT	47.1 ± 11.8	83.1 ± 18.7	9.9 ± 4.0	89.3 ± 37.7	5.9 ± 2.6	51.2 ± 6.6	24.8 ± 6.3	45.1 ± 3.7	263.7 ± 86.3
Temporal WM	CON	50.9 ± 7.6	63.4 ± 11.3	6.9 ± 0.6	49.3 ± 12.3	4.5 ± 0.7	53.3 ± 2.5	21.4 ± 2.2	50.8 ± 1.6	210.6 ± 64.0
	PAT	63.1 ± 21.6	93.5 ± 22.3	10.1 ± 3.6	101.1 ± 48.2	6.4 ± 2.5	49.3 ± 2.2	23.7 ± 7.0	49.1 ± 3.8	282.9 ± 41.1
Occipital WM	CON	40.8 ± 7.5	56.8 ± 12.0	6.2 ± 1.5	40.0 ± 10.8	3.1 ± 0.7	63.2 ± 3.9	19.8 ± 4.3	41.7 ± 1.9	197.3 ± 87.9
	PAT	46.4 ± 11.1	90.2 ± 24.7	7.8 ± 2.3	84.5 ± 31.2	4.4 ± 1.1	56.7 ± 10.5	20.0 ± 7.3	39.7 ± 4.5	316.9 ± 184.7
Deep GM ROIs										
Thalamus	CON	32.8 ± 10.6	98.4 ± 40.8	5.3 ± 1.1	86.2 ± 41.4	3.3 ± 0.6	30.9 ± 5.0	15.4 ± 3.8	24.9 ± 1.9	247.9 ± 138.4
	PAT	49.8 ± 22.0	98.4 ± 43.2	7.5 ± 2.4	114.7 ± 61.8	4.7 ± 1.2	33.7 ± 8.5	18.7 ± 6.8	28.8 ± 5.4	261.0 ± 101.8
Caudate Nucleus	CON	34.8 ± 10.1	114.0 ± 60.6	6.3 ± 2.2	86.2 ± 75.7	3.5 ± 1.0	40.2 ± 11.1	19.9 ± 5.9	21.5 ± 2.7	328.3 ± 128.5
	PAT	45.7 ± 13.2	88.5 ± 58.0	8.5 ± 5.4	83.2 ± 69.8	4.4 ± 2.7	35.4 ± 9.3	27.8 ± 14.0	26.8 ± 7.3	296.9 ± 96.9
Putamen	CON	31.3 ± 10.0	90.0 ± 53.1	4.9 ± 1.4	57.7 ± 31.6	3.2 ± 0.6	48.5 ± 5.2	9.5 ± 3.8	34.0 ± 3.2	320.4 ± 235.2
	PAT	33.8 ± 11.0	171.0 ± 152.5	6.2 ± 2.4	68.7 ± 58.3	4.4 ± 1.9	47.9 ± 3.6	13.5 ± 10.2	36.1 ± 6.0	333.5 ± 328.9

Note: Coefficients of variance (COVs) within regions of interest (ROI) expressed in % of various measures based on all control subjects (n = 15) and all patients (n = 9). All the data represent mean ± standard deviation. No values are provided for corpus callosum and corticospinal tracts, because for probabilistic tracts only the weighted mean is determined, and not the standard deviation, which prevents the calculation of COV. Except for the cerebral white matter, measures of the left ROIs are shown.

Abbreviations: CON, control subjects; DTI, diffusion tensor imaging; FA, fractional anisotropy; FISO, free water fraction; GM, gray matter; IET2, geometrical mean of the intra- and extra-axonal T2; MCR-DIMWI, multi-compartment relaxometry-diffusion informed myelin water imaging; METRICS, multi-echo T2 relaxation imaging with compressed sensing; METRICS[D], postprocessing according to Dvorak et al.,[5]; METRICS[K], postprocessing according to Kumar et al.,[18]; MWF, myelin water fraction; n, number; NDI, neurite density index; NODDI, neurite orientation dispersion and density imaging; ODI, orientation dispersion index; PAT, patients; WM, white matter

WILEY

TABLE 5 Goodness-of-fit measures.

		MCR-DIMWI	METRICS		DTI
		Residuals	FNR	SNR	SSE
WM ROIs					
Cerebral WM	CON	2.08 ± 1.39	572 ± 58	482 ± 58	5.51 ± 1.10
	PAT	2.46 ± 1.56	465 ± 82	408 ± 74	5.17 ± 1.81
Frontal WM	CON	1.54 ± 0.80	555 ± 57	466 ± 56	5.20 ± 1.06
	PAT	2.29 ± 1.67	439 ± 75	385 ± 64	4.68 ± 1.57
Parietal WM	CON	1.81 ± 1.07	617 ± 78	523 ± 77	4.81 ± 1.08
	PAT	1.70 ± 0.62	502 ± 114	438 ± 98	4.64 ± 1.62
Temporal WM	CON	2.32 ± 1.66	589 ± 75	502 ± 76	6.95 ± 1.65
	PAT	2.68 ± 1.65	482 ± 95	423 ± 84	5.69 ± 2.03
Occipital WM	CON	2.56 ± 1.79	618 ± 86	518 ± 90	5.59 ± 1.47
	PAT	2.84 ± 1.78	552 ± 122	483 ± 114	6.11 ± 2.55
Corpus callosum	CON	2.62 ± 1.86	543 ± 53	457 ± 48	13.51 ± 3.28
tract	PAT	3.26 ± 2.42	434 ± 61	381 ± 52	10.43 ± 2.92
Corticospinal	CON	2.88 ± 1.83	500 ± 42	409 ± 39	28.88 ± 5.62
tract	PAT	3.42 ± 1.66	409 ± 52	345 ± 43	29.50 ± 9.19
Deep GM ROIs					
Thalamus	CON	3.44 ± 4.21	398 ± 62	325 ± 56	12.21 ± 5.81
	PAT	3.10 ± 1.72	293 ± 54	237 ± 40	10.58 ± 3.88
Caudate nucleus	CON	2.77 ± 2.36	265 ± 86	232 ± 75	7.87 ± 3.67
	PAT	3.61 ± 3.28	258 ± 52	226 ± 45	8.12 ± 4.84
Putamen	CON	2.37 ± 1.96	566 ± 98	495 ± 85	6.39 ± 3.54
	PAT	2.65 ± 2.12	470 ± 89	419 ± 79	5.58 ± 3.97

Note: Goodness-of-fit measures based on all control subjects ($n = 15$) and all patients ($n = 9$). All the data represent mean $\pm$ standard deviation. Except for the cerebral WM and the tract through the corpus callosum, measures of the left regions of interest (ROIs) are shown. The MCR-DIMWI residuals are normalized values, based on the number of volumes (number of flip angles * number of echo times). The DTI SSE is also adjusted for the number of volumes.
Abbreviations: CON, control subjects; DTI, diffusion tensor imaging; FNR, fit-to-noise ratio; GM, gray matter; MCR-DIMWI, multi-compartment relaxometry-diffusion informed myelin water imaging; METRICS, multi-echo T2 relaxation imaging with compressed sensing; PAT, patients; SNR, signal-to-noise ratio; SSE, sum of squared errors; WM, white matter.

DISCUSSION

In this paper, the applicability of model-based quantitative MRI techniques in a cohort of patients with a variety of leukodystrophies was investigated. Several measures obtained from the described techniques were able to distinguish patients with leukodystrophies from controls. In particular, in WM regions, MWF values derived from both MCR-DIMWI and METRICS were lower in patients than in controls, while relaxation times derived from both techniques were higher in patients, demonstrating the sensitivity to WM damage occurring in leukodystrophies.

The quality assessment indicated a strong agreement between the left and right hemispheres for most quantitative measures. This is expected in controls, but also in leukodystrophy patients, because leukodystrophies typically affect the WM symmetrically. Within-ROI COVs and left-right asymmetries were larger for MWF values than for most other quantitative measures, suggesting a higher variability

of MWF. Still, MWF allowed a clear discrimination between groups as shown by large effect sizes, because the relative differences in MWF values between patients and controls were large. When comparing both MWI techniques, MCR-DIMWI-derived MWF values were more homogeneous within ROIs and showed smaller left-right asymmetries than METRICS-derived MWF values. While our data suggest a lower variability of MWF obtained with MCR-DIMWI, both techniques have a similarly large effect size in differentiating patients and controls.

MWF values of both techniques correlated well, although METRICS-derived MWF was typically higher than MCR-DIMWI-derived MWF. The relation between both MWF values varied per ROI, as also observed in previous papers directly comparing two myelin-sensitive methods.[24-27] Both METRICS-MWF and MCR-DIMWI-MWF showed an increase with age in controls, corresponding to myelination during normal development.[28] This observation has already been described for METRICS.[29] For both techniques, MWF values were lower for patients than for controls. This was expected,

TABLE 6 Laterality indices.

		MCR-DIMWI	METRICS		DTI	NODDI		
		LI MWF	LI MWF	LI IET2	LI FA	LI NDI	LI ODI	LI FISO
WM ROIs								
Frontal WM	CON	0.98 ± 5.25	-1.86 ± 5.37	0.20 ± 0.25	0.09 ± 1.56	0.75 ± 0.60	0.54 ± 1.20	-1.98 ± 24.94
	PAT	2.15 ± 4.50	8.27 ± 46.07	-0.01 ± 0.76	-0.81 ± 2.54	-0.45 ± 3.07	0.40 ± 1.09	-0.79 ± 1.96
Parietal WM	CON	-3.11 ± 5.34	-1.56 ± 6.91	-0.36 ± 0.31	0.42 ± 1.75	0.90 ± 0.76	0.23 ± 1.19	-0.26 ± 32.15
	PAT	-2.41 ± 8.08	3.77 ± 23.37	0.05 ± 0.97	-0.14 ± 2.08	-0.55 ± 2.49	-0.70 ± 1.88	-12.26 ± 32.57
Temporal WM	CON	-6.64 ± 5.64	-4.17 ± 8.72	-0.17 ± 0.40	1.82 ± 2.02	0.39 ± 0.47	-1.36 ± 1.96	24.74 ± 59.13
	PAT	-6.06 ± 8.37	-15.94 ± 35.65	0.21 ± 0.48	0.95 ± 2.26	-0.18 ± 0.90	-1.42 ± 1.80	-0.60 ± 0.96
Occipital WM	CON	-1.98 ± 6.66	-2.06 ± 4.85	-0.18 ± 0.32	1.67 ± 2.64	0.20 ± 1.06	-0.88 ± 1.35	18.57 ± 36.68
	PAT	0.22 ± 9.67	-8.65 ± 11.06	-0.07 ± 0.39	1.10 ± 3.74	0.26 ± 0.54	-1.13 ± 2.24	12.17 ± 25.12
Corticospinal tract	CON	-3.15 ± 4.70	-2.53 ± 5.69	0.24 ± 0.52	-0.14 ± 1.63	-0.33 ± 1.57	0.26 ± 1.15	-2.90 ± 7.63
	PAT	0.18 ± 4.76	-11.23 ± 23.93	0.04 ± 1.17	0.64 ± 3.28	-1.34 ± 2.41	-1.19 ± 3.04	-3.60 ± 7.74
Deep GM ROIs								
Thalamus	CON	-3.60 ± 12.19	3.96 ± 33.41	0.17 ± 1.05	0.63 ± 3.87	0.49 ± 1.02	-0.28 ± 1.67	8.27 ± 25.13
	PAT	-11.63 ± 17.98	-28.47 ± 49.96	-0.10 ± 0.76	-2.25 ± 4.93	0.37 ± 0.92	1.18 ± 3.35	-7.90 ± 20.00
Caudate Nucleus	CON	-5.59 ± 11.02	9.68 ± 42.21	-0.21 ± 1.53	2.84 ± 4.47	0.89 ± 2.52	-0.03 ± 3.20	-0.36 ± 1.38
	PAT	-10.69 ± 10.56	11.11 ± 54.97	1.28 ± 1.56	0.12 ± 3.55	0.25 ± 2.52	0.61 ± 5.89	12.33 ± 35.07
Putamen	CON	-1.85 ± 13.02	1.66 ± 29.16	0.31 ± 0.56	0.33 ± 6.10	0.01 ± 1.21	-0.94 ± 3.56	-0.07 ± 1.40
	PAT	2.58 ± 11.99	-7.61 ± 46.27	0.17 ± 0.73	5.38 ± 9.38	0.75 ± 1.60	-2.76 ± 7.60	-0.17 ± 1.51

Note: Laterality indices (LI, defined as [left−right]/[left+right]) for regions of interest (ROIs) and tracts based on all control subjects ($n = 15$) and all patients ($n = 9$). All the data represent mean $\pm$ standard deviation. LI of the cerebral WM and the tract through the corpus callosum could not be calculated, as the ROIs are bilateral.

Abbreviations: CON, control subjects; DTI, diffusion tensor imaging; FA, fractional anisotropy; FISO, free water fraction; GM, gray matter; IET2, geometrical mean of the intra- and extra-axonal T2; MCR-DIMWI, multi-compartment relaxometry-diffusion informed myelin water imaging; METRICS, multi-echo T2 relaxation imaging with compressed sensing; MWF, myelin water fraction; n, number; NDI, neurite density index; NODDI, neurite orientation dispersion and density imaging; ODI, orientation dispersion index; PAT, patients; WM, white matter.

TABLE 7 Between-scanner variability.

	MCR-DIMWI	Single compartment		METRICS[K]		DTI	NODDI		
	MWF COV	T1 COV	T2* COV	MWF COV	IET2 COV	FA COV	NDI COV	ODI COV	FISO COV
WM ROIs									
Cerebral WM	10.3%	4.5%	1.4%	2.6%	0.1%	1.2%	2.3%	2.5%	65.7%
Frontal WM	13.8%	5.9%	1.7%	4.7%	0.1%	1.6%	3.5%	3.7%	105.3%
Parietal WM	13.4%	8.2%	1.7%	2.6%	0.5%	1.4%	2.0%	5.0%	51.0%
Temporal WM	7.9%	5.7%	0.5%	4.6%	0.3%	2.1%	2.3%	0.7%	171.9%
Occipital WM	8.5%	1.4%	1.3%	5.2%	0.4%	4.1%	1.1%	4.2%	162.6%
Corpus callosum tract	6.9%	5.2%	2.7%	3.5%	0.1%	2.3%	2.0%	2.6%	9.8%
Corticospinal tract	14.4%	4.8%	1.2%	5.8%	0.9%	1.3%	3.3%	2.4%	13.1%
Deep GM ROIs									
Thalamus	22.2%	1.6%	2.3%	15.3%	0.3%	4.1%	3.1%	3.0%	106.6%
Caudate nucleus	31.4%	5.6%	1.2%	21.5%	1.6%	2.3%	3.9%	4.2%	2.1%
Putamen	23.1%	3.8%	3.5%	11.9%	0.4%	3.0%	3.7%	3.5%	1.4%

Note: Coefficient of variance (COV) based on region of interest (ROI)-wise (standard deviation/mean) of measurements performed on three different scanners for one control subject.

Abbreviations: DTI, diffusion tensor imaging; FA, fractional anisotropy; FISO, free water fraction; GM, gray matter; IET2, geometrical mean of the intra- and extra-axonal T2; MCR-DIMWI, multi-compartment relaxometry-diffusion informed myelin water imaging; METRICS, multi-echo T2 relaxation imaging with compressed sensing; METRICS[K], postprocessing according to Kumar et al.[18]; MWF, myelin water fraction; NDI, neurite density index; NODDI, neurite orientation dispersion and density imaging; ODI, orientation dispersion index; WM, white matter.
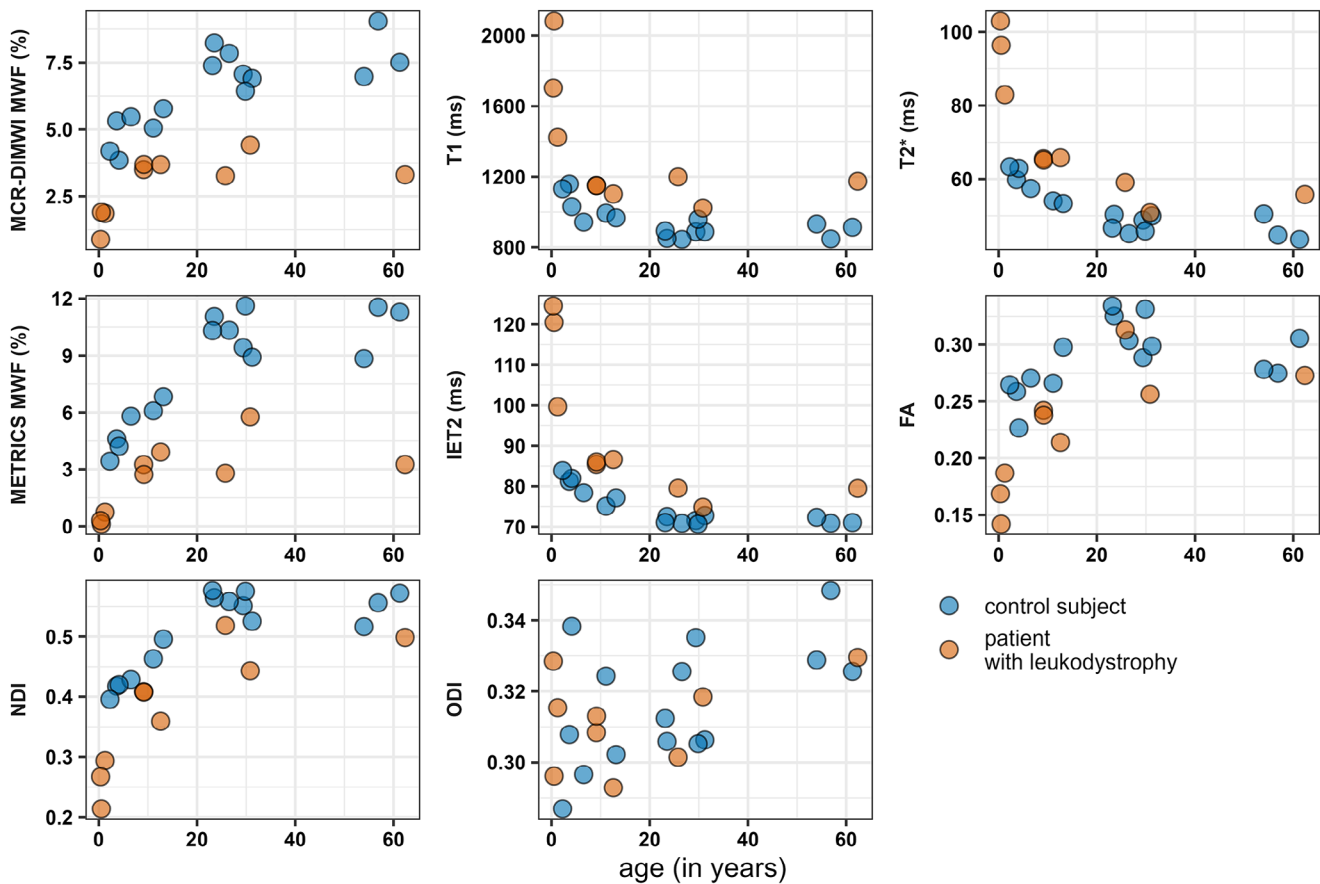
FIGURE 3 Quantitative MRI measures of cerebral white matter shown for patients (orange) and controls (blue) at age of examination. Abbreviations: FA, fractional anisotropy; IET2, geometrical mean of the intra- and extra-axonal T2; MCR-DIMWI, multi-compartment relaxometry-diffusion informed myelin water imaging; METRICS, multi-echo T2 relaxation imaging with compressed sensing; ms, millisecond; MWF, myelin water fraction; NDI, neurite density index; ODI, orientation dispersion index.

as all patients had WM pathology. It should be noted that MWF is a relative value, such that a lower MWF can be caused by a decreased myelin water volume, but also by an increase of nonmyelin water volume. Earlier studies in multiple sclerosis (MS) indicated that the decrease in MWF is mainly driven by the amount of myelin water.[30–32] The MWF reduction in patients with leukodystrophies may be attributed to abnormal myelin, myelin loss, and/or an increase in the spacing of myelin lamellae. These myelin changes also caused the increased relaxation times (T1, T2*, and IET2) observed in the patients. The consistent and clear differences within WM regions between patients and controls indicate the potential of these MWI techniques in WM disorder diagnostics and research. Within deep GM structures, differences between patients and controls were smaller and not significant, possibly partly due to the small group of patients, variety of diseases, low myelin concentration, and possible effects of iron in these regions.[33,34]

The multi-shell DWI data showed expected differences between patients and controls. The effect sizes for NDI and FA were large, but the FA in patients was only significantly lower in the tracts through the corpus callosum, while the NDI was significantly lower in more WM ROIs. These results suggest a higher sensitivity of NDI than of

FA to WM pathology, which has been reported before in patients with Alzheimer's disease and amyotrophic lateral sclerosis.[35,36] The decrease of NDI in abnormal WM has also been consistently reported in MS,[37] likely reflecting axonal damage or loss. FA and NDI were correlated across all ODI ranges in both patients and controls, as also shown for control subjects by Zhang et al.[6] NDI is related to WM pathology, whereas FA can be influenced by pathology and by crossing (healthy) fibers.[6] ODI and FISO showed no consistent differences between patients and controls. This is in line with multiple studies in MS that did not show a difference in ODI when comparing patient NAWM and lesional WM to controls.[37] The lack of differences in FISO in our study contrasts with some studies that showed an increase of FISO in lesional WM compared to NAWM,[38,39] which is typically explained by the breakdown of WM microstructure, resulting in a larger free water fraction. However, a decrease in FISO may also be seen in pathology.[40] The limited observation of differences in FA, ODI, and FISO in the current study may partly be due to variations between patients with different underlying pathologies within this cohort.

MWF values from both MCR-DIMWI and METRICS correlated well with most other measures. This correlation is as expected, because MWF and NDI globally represent myelin and axonal content,
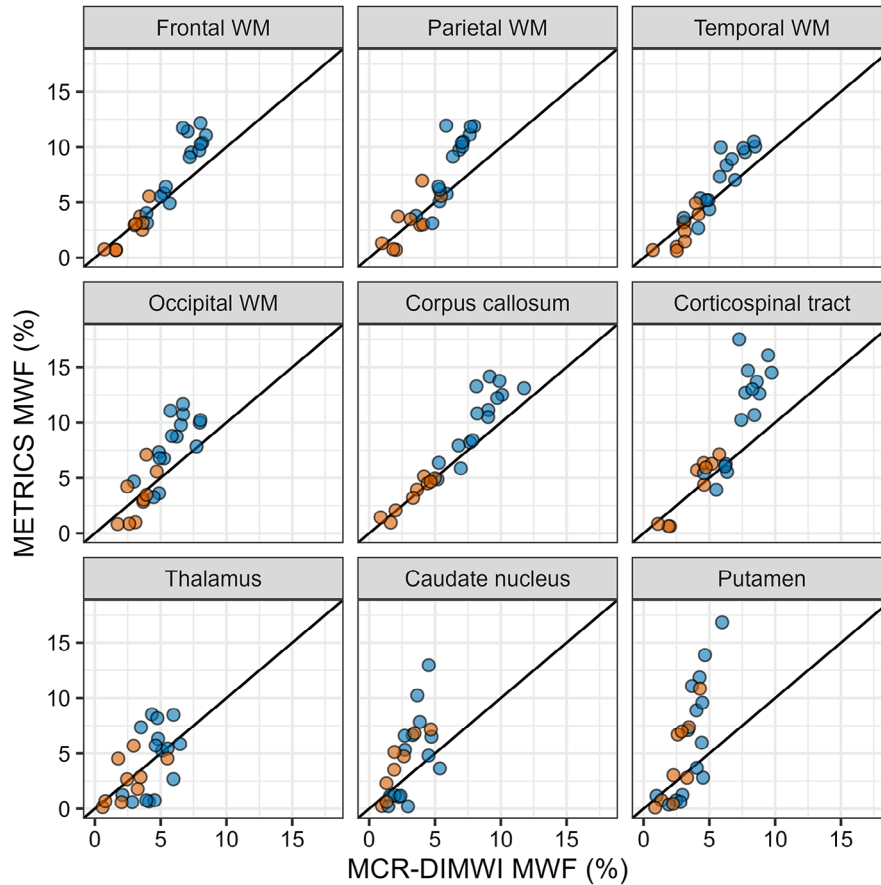
FIGURE 4 Estimated myelin water fraction (MWF) acquired by multi-echo T2 relaxation imaging with compressed sensing (METRICS) versus multi-compartment relaxometry-diffusion informed myelin water imaging (MCR-DIMWI) in nine regions of interest (ROIs, median values per ROI, except for weighted means for the two tracts through the corpus callosum and the corticospinal tract). The identity line is shown. Patients (in orange) show lower MWF values than controls (in blue), with the largest differences seen in the WM ROIs. MWF values of both methods correlate, but on average, METRICS yields higher values than MCR-DIMWI, with larger differences at higher MWF values.
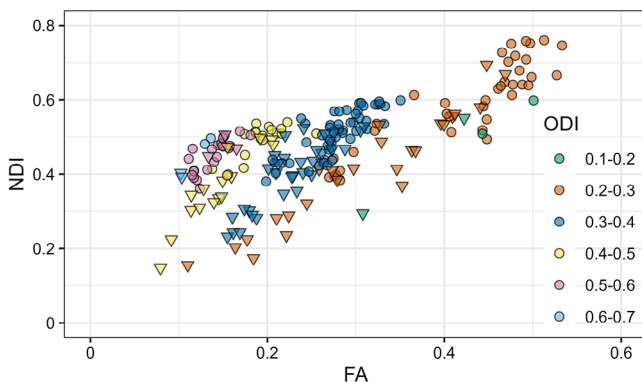
FIGURE 5 Relation between neurite density index (NDI), fractional anisotropy (FA), and orientation dispersion index (ODI) in 9 regions of interest in 15 controls (circles) and 9 patients (triangles). The correlation between FA and NDI depends on the ODI value.

respectively, and leukodystrophies affect both. Model-based quantitative MRI techniques have mainly been used in studies on healthy controls and normal development,[24,26,27,39,40] while patient studies predominantly focused on MS.[32,37] Studies directly comparing techniques are scarce,[24–27] especially in patient settings.[26,39,41,42] The current study investigated the novel whole-brain isotropic techniques METRICS and MCR-DIMWI in relation to NODDI and DTI, both in controls and in patients. The consistent findings in a range of leukodystrophies within our cohort support the robustness of the investigated techniques in WM disorders. Studies in homogeneous patient cohorts for individual leukodystrophies are required to investigate whether model-based microstructural MRI measures correspond to known neuropathological changes and whether they correspond with clinical signs and symptoms.

When interpreting results from biophysical models, it is important to realize that when fitting quantitative measures, fixed constraints or boundary conditions are applied. These constraints are typically derived from healthy adult WM and might not be optimal for use in other physiological contexts or in pathology. For instance, for NODDI, it has been shown that the fixed value of the intrinsic parallel diffusivity of the neurite compartment is suboptimal when analyzing WM in infants or GM, and may lead to biased values in pathology.[43] In addition, NODDI assumes a single T2 value for all compartments, which may

TABLE 8 Quantitative MRI measures.

	Group	MCR-DIMWI	Single compartment		METRICS		DTI	NODDI		
		MWF^c (%)	T1^b (ms)	T2^ab (ms)	MWF^b (%)	IET2^b (ms)	FA^a	NDI^b	ODI^a	FISO
Cerebral WM	CON	6.47^c ± 1.49	949^c ± 96	52^c ± 7	8.28^c ± 2.87	75^c ± 5	0.29^a ± 0.03	0.51^b ± 0.07	0.32 ± 0.02	0.03^b ± 0.03
	PAT	3.64^c ± 0.42	1133^c ± 63	60^c ± 6	3.62^c ± 1.13	82^c ± 5	0.26^a ± 0.03	0.44^b ± 0.06	0.31 ± 0.01	0.01^b ± 0.01
WM ROIs										
Frontal WM	CON	6.54^c ± 1.55	922^c ± 91	53^b ± 7	8.33^c ± 3.08	75^c ± 5	0.29 ± 0.03	0.52^a ± 0.07	0.33 ± 0.02	0.03 ± 0.03
	PAT	3.49^c ± 0.40	1136^c ± 72	63^b ± 7	3.43^c ± 1.09	84^c ± 6	0.25 ± 0.05	0.43^a ± 0.08	0.32 ± 0.01	0.01 ± 0.01
Parietal WM	CON	6.25^b ± 1.25	957^b ± 101	53^b ± 7	8.45^b ± 3.10	74^b ± 4	0.30 ± 0.04	0.53 ± 0.07	0.31 ± 0.02	0.04^a ± 0.03
	PAT	3.80^b ± 1.09	1141^b ± 65	61^b ± 5	4.24^b ± 1.61	80^b ± 4	0.28 ± 0.02	0.46 ± 0.05	0.30 ± 0.01	0.00^a ± 0.00
Temporal WM	CON	6.00^b ± 1.64	941^a ± 105	50^a ± 8	7.18^b ± 2.65	75^b ± 5	0.29 ± 0.02	0.47 ± 0.06	0.31 ± 0.02	0.01 ± 0.02
	PAT	3.42^b ± 0.51	1073^a ± 82	58^a ± 7	3.09^b ± 1.21	82^b ± 4	0.26 ± 0.02	0.43 ± 0.04	0.31 ± 0.03	0.00 ± 0.00
Occipital WM	CON	5.92^b ± 1.42	1006 ± 104	48^c ± 5	8.07^b ± 2.69	74^a ± 5	0.19 ± 0.03	0.48 ± 0.05	0.43^b ± 0.03	0.03 ± 0.03
	PAT	3.73^b ± 0.72	1105 ± 60	56^c ± 6	4.32^b ± 1.68	78^a ± 5	0.20 ± 0.03	0.47 ± 0.04	0.39 ± 0.03	0.03 ± 0.04
Tract through corpus callosum	CON	8.32^b ± 1.80	891^c ± 81	50^c ± 6	10.21^c ± 3.06	75^c ± 3	0.47^c ± 0.03	0.59^b ± 0.06	0.21 ± 0.01	0.11 ± 0.01
	PAT	4.20^c ± 0.63	1165^c ± 46	62^c ± 4	4.40^c ± 0.72	86^c ± 3	0.38^c ± 0.04	0.48^b ± 0.08	0.23 ± 0.01	0.10 ± 0.03
Corticospinal tract	CON	7.50^c ± 1.48	887^c ± 80	49^b ± 7	10.86^a ± 4.39	77^c ± 3	0.47 ± 0.04	0.68^a ± 0.07	0.22 ± 0.01	0.17 ± 0.03
	PAT	4.82^c ± 0.58	1058^c ± 52	59^b ± 6	5.96^a ± 0.91	83^c ± 3	0.42 ± 0.03	0.59^a ± 0.07	0.21 ± 0.01	0.17 ± 0.03
Deep GM ROIs										
Thalamus	CON	4.57 ± 1.19	1048 ± 119	50 ± 10	4.33 ± 3.29	73 ± 5	0.26 ± 0.03	0.48 ± 0.05	0.36 ± 0.02	0.00 ± 0.00
	PAT	3.23 ± 1.27	1107 ± 90	54 ± 8	3.44 ± 1.57	75 ± 4	0.26 ± 0.05	0.46 ± 0.04	0.33 ± 0.04	0.01 ± 0.02
Caudate nucleus	CON	3.19 ± 1.21	1143 ± 130	50 ± 14	4.50 ± 4.04	73 ± 8	0.14 ± 0.02	0.45 ± 0.05	0.56 ± 0.03	0.00 ± 0.00
	PAT	2.65 ± 1.24	1169 ± 104	54 ± 8	4.95 ± 1.87	78 ± 6	0.14 ± 0.05	0.43 ± 0.06	0.53 ± 0.08	0.00 ± 0.00
Putamen	CON	3.64 ± 1.25	1140 ± 117	47 ± 14	6.35 ± 5.46	71 ± 7	0.17 ± 0.04	0.48 ± 0.05	0.51 ± 0.05	0.00 ± 0.00
	PAT	3.13 ± 0.71	1184 ± 79	48 ± 11	6.29 ± 3.01	75 ± 8	0.17 ± 0.03	0.44 ± 0.06	0.48 ± 0.05	0.00 ± 0.00
Group:ROI interaction										
F-value (DF = 152)		11.87^c	24.10^c	2.99^b	8.76^c	6.21^c	8.83^c	11.73^c	1.57	2.69^b
Effect size (η_p^2)		0.38	0.56	0.14	0.32	0.25	0.32	0.38	0.08	0.12

Note: Quantitative MRI measures per group based on all control subjects ($n = 15$) and patients >2 years ($n = 6$). All the data represent mean ± standard deviation unless otherwise indicated. Symbols a, b, and c on the top row indicate p-values of the effect of group for all nine WM and deep GM regions of interest (ROIs) in total. p-values per ROI are corrected for multiple testing. Cerebral WM was tested separately. [a]: $p < 0.05$; [b]: $p < 0.01$; [c]: $p < 0.001$.

Abbreviations: CON, healthy controls; DTI, diffusion tensor imaging; FA, fractional anisotropy; FISO, free water fraction; GM, gray matter; IET2, geometrical mean of the intra- and extra-axonal T2; MCR-DIMWI, multi-compartment relaxometry-diffusion informed myelin water imaging; METRICS, multi-echo T2 relaxation imaging with compressed sensing; ms, millisecond; MWF, myelin water fraction; n, number; NDI, neurite density index; NODDI, neurite orientation dispersion and density imaging; ODI, orientation dispersion index; PAT, patients with leukodystrophy; WM, white matter.
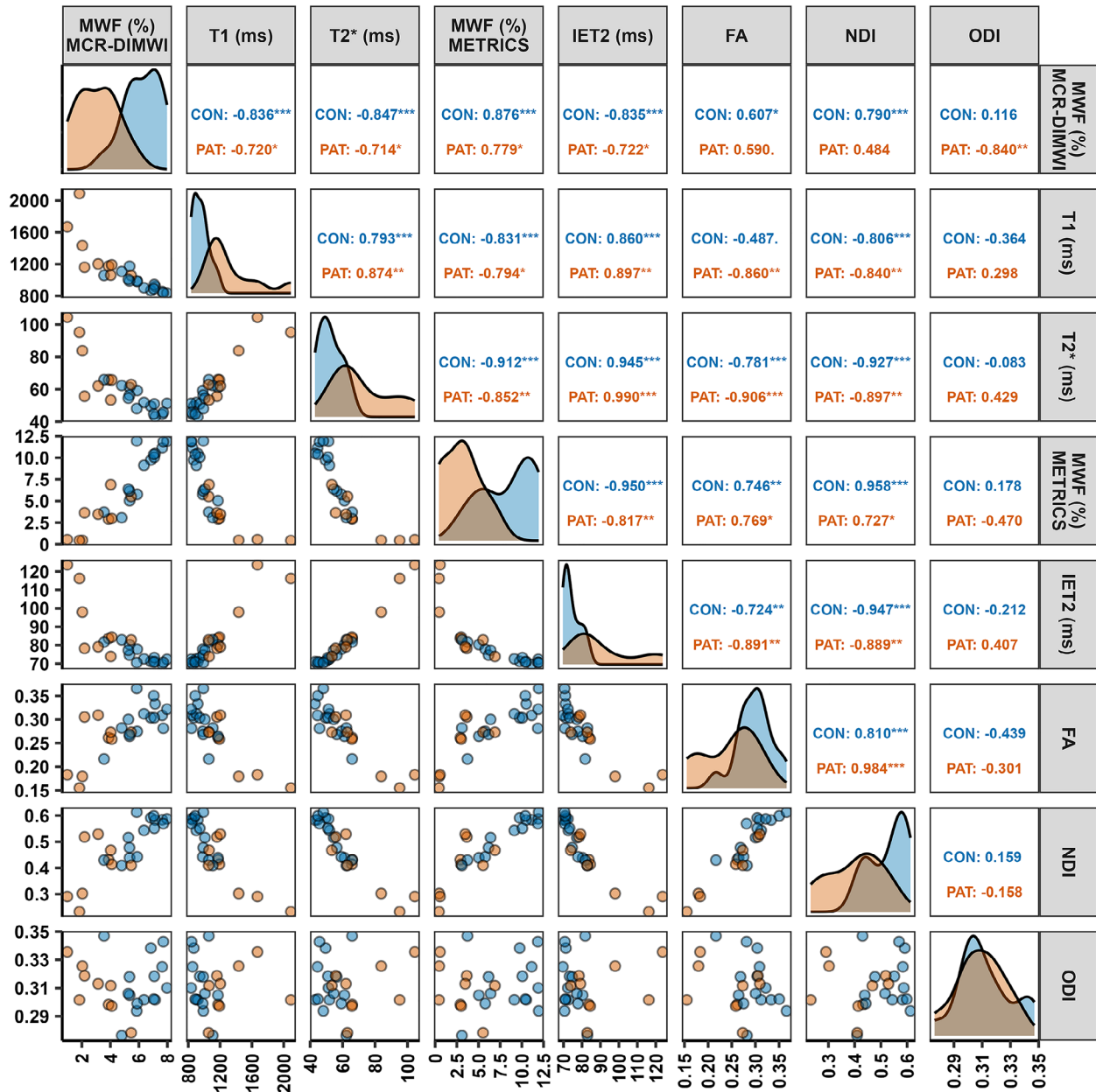
FIGURE 6 Distribution histograms (diagonal panels), scatterplots (lower panels), and Pearson correlation coefficients (upper panels) between various quantitative measures in patients ($n = 9$, orange) and controls ($n = 15$, blue) of the left parietal WM. *p<.05; **p<.01; ***p<.001. Except for orientation dispersion index (ODI), correlations were observed between multi-compartment relaxometry-diffusion informed myelin water imaging (MCR-DIMWI)-, multi-echo T2 relaxation imaging with compressed sensing (METRICS)-, and multi-shell diffusion-weighted imaging-derived measures, both in patients and in controls.

Abbreviations: FA, fractional anisotropy; IET2, geometrical mean of the intra- and extra-axonal T2; ms, millisecond; MWF, myelin water fraction; NDI, neurite density index.

lead to inaccurate FISO values, and an overestimation of NDI. Adapted NODDI models have recently been described,[44,45] and a comparison of these NODDI models will be of interest for future analyses in the leukodystrophy patients. Similar issues may occur in MWI techniques, which also rely on assumptions regarding relaxation times and magnetic susceptibility of myelin,[4] or on the range of T2-relaxation times of myelin water and intra- and extra-axonal water.[5] Constraints are

needed to limit the number of variables, but potential biases need to be considered.

The analysis pipeline we developed can be used with only a 3D structural image and DTI sequence for segmentation purposes and registration by dtitk, respectively. The quantitative sequences multi-shell DWI, MGRE-VFA, and METRICS can be processed independently. We used multi-shell DWI data in the processing of

MCR-DIMWI to improve the robustness of the estimation, but this is not mandatory.[4]

Some strengths and limitations depend on the applied sequence. A strength of METRICS is the option to visualize the T2 distributions within selected ROIs, showing possible variations of T2 values of water compartments depending on the pathology. If motion occurs, the fitting quality of METRICS may be lower, as there is currently no option for motion correction, and the sequence has 9 minutes 27 seconds acquisition time. In MGRE-VFA, coregistration is performed between flip angle sets of 1 minute 26 seconds, but not between TE volumes, which makes the method less sensitive to motion. The multi-shell DWI postprocessing is most robust to motion, with slice-to-volume registration and outlier replacement as performed by eddy. Reliability of the measures is partly dependent on the ROI. In MGRE-VFA, susceptibility artifacts at the border of orbitofrontal areas lead to unreliable values. Voxels with these unreliable values can be determined objectively, based on a high normalized residual, but need to be excluded and are, therefore, lacking in the analyses. This effect could potentially be decreased by acquiring data with a higher spatial resolution, at the expense of scan time and SNR. In METRICS, artifacts were typically CSF- or blood flow-related, which did not overlap with the currently analyzed ROIs. Relatively high METRICS-derived MWF values were observed in deep GM ROIs, likely due to the presence of iron that shortens T2 relaxation times, which increases the fraction being modeled as myelin water.[46]

The spatial resolution of the multi-shell DWI, MGRE-VFA, and METRICS sequences was relatively low, with isotropic 2.5-mm voxels. This yields images with high SNR while keeping acquisition times feasible for clinical application. Although this low resolution prevents the detection of very small, localized abnormalities, this is hardly an issue in leukodystrophies, in which large WM areas are affected. In disorders with smaller size lesions, such as MS, a higher spatial resolution may be necessary. Further shortening of the acquisition time is possible in MGRE-VFA by acquiring only a selection of the current seven flip angles, which has a limited effect on the robustness,[8] and in METRICS by drastically increasing the undersampling acceleration using the CALIPR framework.[47] In the current study, we used three different scanners to scan control subjects, while patients were only scanned on one of the three. The acquisition parameters of the multi-compartment relaxometry techniques were identical on all scanners, and small differences existed only for multi-shell DWI. The between-scanner variation that we estimated for one subject had the same order of magnitude as previously reported for within-scanner repeatability of METRICS-MWF and IET2.[5] The between-scanner variation of MCR-DIMWI-MWF was larger than for METRICS-MWF. Differences in radiofrequency pulses between the scanners may have some influence on MCR-DIMWI-MWF, partly causing higher variation.[8] For all measures in the control subject, differences between scanners were small compared to the observed differences between patients and controls.

When studying rare diseases, low patient numbers are inevitable. Additionally, the variety of disorders with differentially affected WM in different regions probably prevented the detection of all potential (significant) differences between the patient and control groups. However, MWF and relaxation times differed significantly, and trends for lower FA or NDI in the patients could be recognized in all WM regions, even if significance was not reached for those variables. Because of developmental changes, control values of children under 2 years of age are required. Control subjects under the age of 2 years were not included, which limited the comparison of the three youngest patients in this age range. Based on the developed analysis pipeline and building on this proof-of-concept, studies investigating quantitative measures in homogeneous leukodystrophy cohorts in relation to clinical signs and symptoms are currently ongoing.

MCR-DIMWI, METRICS, and NODDI provide whole-brain maps reflecting microstructural components and can distinguish patients with various genetic WM disorders from controls with large effect sizes. To ensure reasonable acquisition times but a high SNR, a relatively low spatial resolution can be accepted, which is sufficient for disorders with extensively affected WM. Future studies incorporating clinical measures from leukodystrophy patients can explore the use of model-based quantitative MRI techniques in monitoring disease progression, as well as treatment effects.

ORCID

Menno D. Stellingwerff https://orcid.org/0000-0001-8881-4989
Murtadha L. Al-Saady https://orcid.org/0000-0002-8246-8963
Kwok-Shing Chan https://orcid.org/0000-0001-8427-169X
Adam Dvorak https://orcid.org/0000-0001-6107-5610
José P. Marques https://orcid.org/0000-0001-8157-8864
Shannon Kolind https://orcid.org/0000-0003-1362-1968
Stefan D. Roosendaal https://orcid.org/0000-0002-3763-4774
Nicole I. Wolf https://orcid.org/0000-0003-1721-0728
Frederik Barkhof https://orcid.org/0000-0003-3543-3706

Marjo S. van der Knaap https://orcid.org/0000-0001-8912-0954
Petra J. W. Pouwels https://orcid.org/0000-0001-8430-0606

REFERENCES

1. van der Knaap MS, Bugiani M. Leukodystrophies: a proposed classification system based on pathological changes and pathogenetic mechanisms. Acta Neuropathol. 2017;134:351–82.
2. Stellingwerff MD, Pouwels PJW, Roosendaal SD, Barkhof F, van der Knaap MS. Quantitative MRI in leukodystrophies. Neuroimage Clin. 2023;38:103427.
3. van der Weijden CWJ, Biondetti E, Gutmann IW, et al. Quantitative myelin imaging with MRI and PET: an overview of techniques and their validation status. Brain. 2023;146:1243–66.
4. Chan KS, Marques JP. Multi-compartment relaxometry and diffusion informed myelin water imaging—promises and challenges of new gradient echo myelin water imaging methods. Neuroimage. 2020;221:117159.
5. Dvorak AV, Wiggermann V, Gilbert G, et al. Multi-spin echo T2 relaxation imaging with compressed sensing (METRICS) for rapid myelin water imaging. Magn Reson Med. 2020;84:1264–79.
6. Zhang H, Schneider T, Wheeler-Kingshott CA, Alexander DC. NODDI: practical in vivo neurite orientation dispersion and density imaging of the human brain. Neuroimage. 2012;61:1000–1016.
7. Caruyer E, Lenglet C, Sapiro G, Deriche R. Design of multishell sampling schemes with uniform coverage in diffusion MRI. Magn Reson Med. 2013;69:1534–40.
8. Chan KS, Chamberland M, Marques JP. On the performance of multi-compartment relaxometry for myelin water imaging (MCR-MWI)—test-retest repeatability and inter-protocol reproducibility. Neuroimage. 2023;266:119824.
9. Nehrke K, Börnert P. DREAM—a novel approach for robust, ultrafast, multislice B1 mapping. Magn Reson Med. 2012;68:1517–26.
10. Li X, Morgan PS, Ashburner J, Smith J, Rorden C. The first step for neuroimaging data analysis: DICOM to NIfTI conversion. J Neurosci Methods. 2016;264:47–56.
11. Billot B, Greve DN, Puonti O, et al. SynthSeg: segmentation of brain MRI scans of any contrast and resolution without retraining. Med Image Anal. 2023;86:102789.
12. Avants BB, Tustison NJ, Song G, Cook PA, Klein A, Gee JC. A reproducible evaluation of ANTs similarity metric performance in brain image registration. Neuroimage. 2011;54:2033–44.
13. Andersson JL, Skare S, Ashburner J. How to correct susceptibility distortions in spin-echo echo-planar images: application to diffusion tensor imaging. Neuroimage. 2003;20:870–88.
14. Andersson JL, Sotiropoulos SN. An integrated approach to correction for off-resonance effects and subject movement in diffusion MR imaging. Neuroimage. 2016;125:1063–78.
15. Hernandez-Fernandez M, Reguly I, Jbabdi S, Giles M, Smith S, Sotiropoulos SN. Using GPUs to accelerate computational diffusion MRI: from microstructure estimation to tractography and connectomes. Neuroimage. 2019;188:598–615.
16. Deoni SC, Rutt BK, Peters TM. Rapid combined T1 and T2 mapping using gradient recalled acquisition in the steady state. Magn Reson Med. 2003;49:515–26.
17. Prasloski T, Madler B, Xiang QS, MacKay A, Jones C. Applications of stimulated echo correction to multicomponent T2 analysis. Magn Reson Med. 2012;67:1803–14.
18. Kumar D, Hariharan H, Faizy TD, et al. Using 3D spatial correlations to improve the noise robustness of multi component analysis of 3D multi echo quantitative T2 relaxometry data. Neuroimage. 2018;178:583–601.
19. Zhang H, Avants BB, Yushkevich PA, et al. High-dimensional spatial normalization of diffusion tensor images improves the detection of white matter differences: an example study using amyotrophic lateral sclerosis. IEEE Trans Med Imaging. 2007;26:1585–97.
20. Zhang H, Yushkevich PA, Alexander DC, Gee JC. Deformable registration of diffusion tensor MR images with explicit orientation optimization. Med Image Anal. 2006;10:764–85.
21. Al-Saady ML, Wolf NI, Pouwels PJW. Segmentation of intrinsically very low contrast magnetic resonance brain images using tensor-based DTI registration. Neuroimage: Reports. 2022;2:100120.
22. Zhang S, Arfanakis K. Evaluation of standardized and study-specific diffusion tensor imaging templates of the adult human brain: template characteristics, spatial normalization accuracy, and detection of small inter-group FA differences. Neuroimage. 2018;172:40–50.
23. Cohen J. Statistical power analysis for the behavioral sciences, 2nd ed. Hillsdale, NJ: Erlbaum; 1988.
24. Alonso-Ortiz E, Levesque IR, Pike GB. Multi-gradient-echo myelin water fraction imaging: comparison to the multi-echo-spin-echo technique. Magn Reson Med. 2018;79:1439–46.
25. Geeraert BL, Lebel RM, Mah AC, et al. A comparison of inhomogeneous magnetization transfer, myelin volume fraction, and diffusion tensor imaging measures in healthy children. Neuroimage. 2018;182:343–50.
26. Choi JY, Jeong IH, Oh SH, et al. Evaluation of normal-appearing white matter in multiple sclerosis using direct visualization of short transverse relaxation time component (ViSTa) myelin water imaging and gradient echo and spin echo (GRASE) myelin water imaging. J Magn Reson Imaging. 2019;49:1091–98.
27. Zhang J, Kolind SH, Laule C, MacKay AL. Comparison of myelin water fraction from multiecho T2 decay curve and steady-state methods. Magn Reson Med. 2015;73:223–32.
28. Yeatman JD, Wandell BA, Mezer AA. Lifespan maturation and degeneration of human brain white matter. Nat Commun. 2014;5:4932.
29. Dvorak AV, Swift-LaPointe T, Vavasour IM, et al. An atlas for human brain myelin content throughout the adult life span. Sci Rep. 2021;11:269.
30. Laule C, Vavasour IM, Moore GR, et al. Water content and myelin water fraction in multiple sclerosis. A T2 relaxation study. J Neurol. 2004;251:284–93.
31. Meyers SM, Kolind SH, MacKay AL. Simultaneous measurement of total water content and myelin water fraction in brain at 3T using a T(2) relaxation based method. Magn Reson Imaging. 2017;37:187–94.
32. Laule C, Moore GRW. Myelin water imaging to detect demyelination and remyelination and its validation in pathology. Brain Pathol. 2018;28:750–64.
33. Gutmann DH, Zackai EH, McDonald-McGinn DM, Fischbeck KH, Kamholz J. Oculodentodigital dysplasia syndrome associated with abnormal cerebral white matter. Am J Med Genet. 1991;41:18–20.
34. Svingen L, Goheen M, Godfrey R, et al. Late diagnosis and atypical brain imaging of Aicardi-Goutieres syndrome: are we failing to diagnose Aicardi-Goutieres syndrome-2? Dev Med Child Neurol. 2017;59:1307–11.
35. Broad RJ, Gabel MC, Dowell NG, et al. Neurite orientation and dispersion density imaging (NODDI) detects cortical and corticospinal tract degeneration in ALS. J Neurol Neurosurg Psychiatry. 2019;90:404–11.
36. Fu X, Shrestha S, Sun M, et al. Microstructural white matter alterations in mild cognitive impairment and Alzheimer's disease: study based on Neurite Orientation Dispersion and Density Imaging (NODDI). Clin Neuroradiol. 2020;30:569–79.
37. Alotaibi A, Podlasek A, AlTokhis A, Aldhebaib A, Dineen RA, Constantinescu CS. Investigating microstructural changes in white matter in multiple sclerosis: a systematic review and meta-analysis of neurite orientation dispersion and density imaging. Brain Sci. 2021;11:1151.
38. Schneider T, Brownlee W, Zhang H, Ciccarelli O, Miller DH, Wheeler-Kingshott CG. Sensitivity of multi-shell NODDI to multiple sclerosis white matter changes: a pilot study. Funct Neurol. 2017;32:97–101.
39. Hagiwara A, Kamagata K, Shimoji K, et al. White matter abnormalities in multiple sclerosis evaluated by quantitative synthetic MRI, diffusion tensor imaging, and neurite orientation dispersion and density imaging. AJNR Am J Neuroradiol. 2019;40:1642–48.

40. Martin P, Hagberg GE, Schultz T, et al. T2-pseudonormalization and microstructural characterization in advanced stages of late-infantile metachromatic leukodystrophy. Clin Neuroradiol. 2020;31: 969–80.

41. Elkady AM, Wu Z, Leppert IR, Arnold DL, Narayanan S, Rudko DA. Assessing the differential sensitivities of wave-CAIPI ViSTa myelin water fraction and magnetization transfer saturation for efficiently quantifying tissue damage in MS. Mult Scler Relat Disord. 2021;56:103309.

42. Wiggermann V, Endmayr V, Hernandez-Torres E, et al. Quantitative magnetic resonance imaging reflects different levels of histologically determined myelin densities in multiple sclerosis, including remyelination in inactive multiple sclerosis lesions. Brain Pathol. 2023;33:e13150.

43. Guerrero JM, Adluru N, Bendlin BB, et al. Optimizing the intrinsic parallel diffusivity in NODDI: an extensive empirical evaluation. PLoS One. 2019;14:e0217118.

44. Alsameen MH, Gong Z, Qian W, et al. C-NODDI: a constrained NODDI model for axonal density and orientation determinations in cerebral white matter. Front Neurol. 2023;14:1205426.

45. Bouyagoub S, Dowell NG, Hurley SA, Wood TC, Cercignani M. Over-estimation of CSF fraction in NODDI: possible correction techniques and the effect on neurite density and orientation dispersion measures. *24th Annual Meeting of the International Society for Magnetic Resonance in Medicine Singapore.* 2016.

46. Birkl C, Birkl-Toeglhofer AM, Endmayr V, et al. The influence of brain iron on myelin water imaging. Neuroimage. 2019;199:545–52.

47. Dvorak AV, Kumar D, Gilbert G, et al. The CALIPR framework comprehensively improves acquisition, reconstruction & analysis of multi-component relaxation imaging. *Proceedings Joint Annual Meeting ISMRM-ESMRMB 2022.* 2022.

How to cite this article: Stellingwerff MD, Al-Saady ML, Chan K-S, et al. Applicability of multiple quantitative magnetic resonance methods in genetic brain white matter disorders. J Neuroimaging. 2023;1–17. https://doi.org/10.1111/jon.13167